Supplement of Atmos. Chem. Phys., 21, 6663–6680, 2021
https://doi.org/10.5194/acp-21-6663-2021-supplement

Atmospheric Chemistry and Physics
Open Access

Supplement of

Linking global terrestrial CO_2 fluxes and environmental drivers: inferences from the Orbiting Carbon Observatory 2 satellite and terrestrial biospheric models

Zichong Chen et al.

Correspondence to: Zichong Chen (zchen74@jhu.edu)

S1. Additional detail on the regression and inverse model (GIM) using OCO-2 observations

S1.1 Specific inverse model setup

We estimate both the fluxes ($\boldsymbol{s}$, where $\boldsymbol{s} = \mathbf{X}\boldsymbol{\beta} + \boldsymbol{\zeta}$) and the drift coefficients ($\boldsymbol{\beta}$) by minimizing the GIM cost function (e.g., *Kitanidis and Vomvoris,* 1983; *Kitanidis,* 1995*; Michalak et al*., 2004):

$$L_{s,\beta} = \frac{1}{2}(\boldsymbol{z} - h(\boldsymbol{s}))^{\boldsymbol{T}}\mathbf{R}^{-\mathbf{1}}(\boldsymbol{z} - h(\boldsymbol{s})) + \frac{1}{2}(\boldsymbol{s} - \mathbf{X}\boldsymbol{\beta})^{\boldsymbol{T}}\mathbf{Q}^{-\mathbf{1}}(\boldsymbol{s} - \mathbf{X}\boldsymbol{\beta}) \quad \text{(S1)}$$

where $\boldsymbol{s}$ (dimensions $m \times 1$) is a vector of unknown fluxes and $\boldsymbol{z}$ (dimensions $n \times 1$) the observations. We pass the fluxes ($\boldsymbol{s}$) through an atmospheric model ($h()$) to simulate atmospheric CO_2 ($h(\boldsymbol{s})$). In this study, $\mathbf{X}$ (dimensions $m \times p$) is a matrix of environmental drivers, and $\boldsymbol{\beta}$ (dimensions $p \times 1$) are unknown drift coefficients that scale the individual columns in $\mathbf{X}$ to best match the observations ($\boldsymbol{z}$)**.** Collectively, $\mathbf{X}\boldsymbol{\beta}$ is referred to as the deterministic model. Furthermore, $\boldsymbol{s} - \mathbf{X}\boldsymbol{\beta}$ represents spatiotemporal patterns in CO_2 fluxes ($\boldsymbol{s}$) that are implied by the atmospheric observations ($\boldsymbol{z}$) but not captured by the deterministic model ($\mathbf{X}\boldsymbol{\beta}$). In the manuscript, we refer to this component as the stochastic component ($\boldsymbol{\zeta}$).

The inverse model includes two covariance matrices; $\mathbf{R}$ (dimensions $n \times n$) and $\mathbf{Q}$ (dimensions $m \times m$). The covariance matrix $\mathbf{R}$ describes $\boldsymbol{z} - h(\boldsymbol{s})$, referred to here as the model-data mismatch errors. These errors include errors from the atmospheric measurements and from the transport model; in brief, the measurement errors are computed as the variances for 10-s averages by summing the inverse variances of all the soundings within the span of that 10-s average (e.g., *Crowell et al*., 2019), and the model errors consider errors from the model transport and representativeness (e.g., *Basu et al*., 2018); the model-data mismatch errors are the quadrature sum of the measurement errors and model errors. The covariance matrix $\mathbf{Q}$ prescribes the variances and spatiotemporal covariances of the stochastic component ($\boldsymbol{\zeta}$) and includes both diagonal and off-diagonal elements. Specifically, we use Restricted Maximum Likelihood (RML; e.g., *Kitanidis,* 1997; *Gourdji et al*., 2012; *Miller et al*., 2016) to estimate the covariance parameters for $\mathbf{Q}$, including the variance of $\mathbf{Q}$ (referred to as σ_Q^2), the decorrelation length (l), and the decorrelation time (t). We iteratively optimize these covariance parameters using flux estimates for years 2015 to 2018 from CarbonTracker (CT2019; *Peters et al*., 2007, *Jacobson et al*., 2020; https://www.esrl.noaa.gov/gmd/ccgg/carbontracker/). In this study we assume that the spatiotemporal properties of CO_2 fluxes from CT2019 are a reasonable proxy for the covariance parameters that are used in the GIM. Refer to *Mueller et al*. (2008) and *Gourdji et al*. (2008, 2010, 2012) for more detail on this proxy approach to estimating covariance parameters in the inverse model setup. We re-grid the flux estimates from CT2019 to daily, 4º (latitude) by 5º (longitude) resolutions, consistent with the GEOS-Chem model grid and the temporal resolution of the stochastic component (ζ) of the GIM. We optimize these covariance parameters using an exponential covariance model (e.g., *Mueller et al*., 2008; *Gourdji et al*., 2008, 2010, 2012) for land and ocean, respectively. We specifically estimate a variance of 0.31 (μmol m^{-2} s^{-1})^2 for terrestrial regions and 0.014 (μmol m^{-2} s^{-1}) for the ocean. We further estimate a decorrelation length parameter of 1460 km for land and 4678 km for ocean and a correlation time parameter of 5.1 days for land and 8.6 days for the ocean. These values have a similar magnitude to an existing global GIM study (*Gourdji et al*., 2008).

After estimating the covariance matrix parameters, we then estimate the CO_2 fluxes by iteratively minimizing Eq. S1 using the Limited-memory Broyden-Fletcher-Goldfarb-Shanno algorithm (L-BFGS, *Liu and Nocedal*, 1989). *Miller et al* (2020) provides detail on this iterative approach to minimize Eq. S1.

S1.2 Initial condition of atmospheric CO_2 and model spin-up

We first create an initial condition of atmospheric CO_2 mole fractions for 1 Sept., 2012 based on NOAA's Carbon Tracker (CT) product, and use CO_2 fluxes from CT to run GEOS-Chem forward for two years until 1 Sept., 2014 when the inverse modeling begins; we run the CT fluxes through GEOS-Chem for two years to ensure that the CO_2 mixing ratios are consistent with the GEOS-Chem model grid, and therefore to minimize potential spin-up artifacts due to model transport. We then run the inverse model starting from 1 Sept., 2014, but we consider the result from 2014 as part of an initial model spin-up period and do not use it for analysis. This setup for the initial condition and spin-up is identical to that used in *Miller et al*. (2018).

S2. Additional detail on the setup of anthropogenic emissions, ocean fluxes, and biomass burning

We combine fossil fuel emissions from ODIAC, biomass burning fluxes from GFED, and oceanic fluxes from ECCO-Darwin in a single column of $\mathbf{X}$ and estimate a single coefficient (β)

for all three sources in all regions of the globe. This column of combined fluxes is selected using the BIC and is included within the inverse model. Furthermore, we estimate a coefficient ($\boldsymbol{\beta}$) of 0.97 to 1.05 (depending on the year and simulation) for this column of **X**. A scaling factor near one indicates that the overall, cumulative magnitude of these sources is consistent with OCO-2 observations.

We do not estimate separate coefficients ($\boldsymbol{\beta}$) for fossil fuel emissions from ODIAC, biomass burning fluxes from GFED, and oceanic fluxes from ECCO-Darwin separately because current OCO-2 observations have limited ability to constrain patterns in these different source types. We conduct a sensitivity test in which we use three individual columns in **X** to represent ODIAC, GFED, and ECCO-Darwin, respectively; we then re-run model selection using this setup for **X**. We select ODIAC but not GFED or ECCO-Darwin in this sensitivity test. This result suggests that ODIAC helps describe enough variability in atmospheric observations to be selected using BIC; by contrast, GFED or ECCO-Darwin alone do not help reproduce OCO-2 observations more than the penalty term (Eq. 2) in the BIC and therefore are not selected. The average atmospheric XCO_2 enhancement due to GFED emissions and ECCO-Darwin fluxes are 0.19 and -0.31ppm, respectively. These enhancements are small relative to emissions from ODIAC (2.70 ppm), a possible explanation of why ocean and biomass burning fluxes are not selected in this sensitivity test.

S3. Scaled temperature function

Most terrestrial biosphere models (TBMs) estimate CO_2 fluxes as a nonlinear or piecewise function of temperature (e.g., *Heskel et al*., 2016; *Dayalu et al*., 2018). In this study, we use a scaled function of temperature from the Vegetation Photosynthesis and Respiration Model (VPRM, *Mahadevan et al*., 2008; *Dayalu et al*., 2018) as an environmental driver in the inverse model (in **X**, Eq. 1). This function peaks at the optimal temperature for photosynthesis and declines at higher and lower temperatures:

$$\boldsymbol{T_{scale}} = \frac{(\boldsymbol{T_{air}}-\boldsymbol{T_{min}})(\boldsymbol{T_{air}}-\boldsymbol{T_{max}})}{(\boldsymbol{T_{air}}-\boldsymbol{T_{min}})(\boldsymbol{T_{air}}-\boldsymbol{T_{max}})-(\boldsymbol{T_{air}}-\boldsymbol{T_{opt}})^2} \quad \text{(S2)}$$

The scaled temperature ($\boldsymbol{T_{scale}}$) is calculated based on a minimum ($\boldsymbol{T_{min}}$ = 0 ^{o}C) and maximum ($\boldsymbol{T_{max}}$ = 40 ^{o}C) temperature threshold and an optimal temperature ($\boldsymbol{T_{opt}}$) for photosynthesis which is set for each biome. In this study, we follow existing literature (*Mahadevan et al*., 2008; *Luus et al*., 2017; *Dayalu et al*., 2018) and set an optimal temperature of 15 ^{o}C for tundra and boreal biomes, and 20 ^oC for temperate, tropical, and desert/shrubland biomes. An example of scaled temperature as a function of air temperature over the temperate forest biome is illustrated in Fig. S1.

S4. Comparisons against XCO_2 observations, against aircraft-based measurements, and against TCCON measurements

S4.1 Comparisons against XCO_2 observations

We simulate posterior atmospheric CO_2 concentrations for years 2015 through 2018 by passing the posterior CO_2 fluxes ($\hat{\boldsymbol{s}}$) through the atmospheric transport model ($h(\hat{\boldsymbol{s}})$).; we then compare the modeled XCO_2 against observed XCO_2. Fig. S2 displays the model-data XCO_2 comparisons for years 2015 through 2018. Across the study years, the model-data biases are small and range from -0.15 to -0.08 ppm. Furthermore, the root mean squared error (RMSE) ranges from 1.03 to 1.16 ppm, depending upon the year. These errors are similar to the model-data mismatch errors specified in the inverse model (0.98 ± 0.31 ppm), indicating that the covariance matrix **R** is a reasonable estimate of the actual residuals. In addition, the model-data fit is consistent among all years of the inverse modeling results; the model-data residuals are similar from one year to another and do not display any trend.

S4.2 Comparisons against aircraft-based measurements

We evaluate the inverse model estimates against aircraft-based measurements included in the NOAA ObsPack (version 2.0, NOAA Carbon Cycle Group Obspack team, 2018; *Masarie et al*., 2014). These measurements include vertical profiles collected from NOAA regular aircraft sites (*Sweeney et al*., 2015), from the National Institute for Space Research (INPE), and from the Atmospheric Tomography Mission campaign (ATom, *Wofsy et al*., 2018). Table S2 displays a full list of the aircraft sites and campaign used in this study. Note that we remove a few outlier data points from this comparison, defined as differences between posterior CO_2 and aircraft measurements that are larger than 30 ppm; these outliers may indicate very heavy local influence (e.g., *Chevallier et al*., 2019).

Figs. S3-S6 displays site-level comparisons against aircraft measurements collected from NOAA aircraft sites and from INPE sites. We find that from one year to another, the model-data biases and the RMSEs show similar magnitudes and patterns. The model-data differences over middle latitudes are generally small and become larger across high latitudes. There are few OCO-2 observations in high latitude regions, a possible reason why the error statistics are larger in high latitude regions like Alaska. Furthermore, the resolution of the global GOES-Chem model (4^{o} latitude × 5^{o} longitude) may introduce additional uncertainties in comparisons with aircraft point data that show substantial spatial heterogeneity (e.g, *Crowell et al*., 2019). With that said, these site-level comparisons are broadly consistent with previous studies (*Chevallier et al*. 2019; *Liu et al*., 2020) in which the authors used aircraft measurements to evaluate inverse model estimates from GOSAT and OCO-2 satellites. Note that the sites available for comparison differs slightly from one year to another; for example, there are not any available aircraft measurements at RBA-B and ALF sites over South America for year 2018 (Fig. S6).

Furthermore, Fig. S7 shows grid-scale (4^{o} latitude × 5^{o} longitude) comparisons against the ATom airborne campaigns. ATom aircraft measurements were collected from August 2016 to May 2018 over Pacific and Atlantic oceans. Within each grid box, we average available aircraft measurements for comparison. We find that over most of the grid boxes the residuals between modeled and observed CO_2 are within 1.0 ppm; these residuals are similar in magnitude to the model-data mismatch errors specified in the inverse model, further indicating a good match between the **R** covariance matrix and actual model-data residuals. In addition, the model-data residuals are smallest over ocean and are larger over land. These patterns in the residuals are broadly consistent with a recent study that employed GOSAT and OCO-2 satellite observations (*Liu et al*., 2020).

Overall, the agreement between posterior CO_2 and various aircraft measurements confirms the conclusion that there are no major biases in the GIM flux estimates using OCO-2.

S.4.3 Comparisons against TCCON measurements

We sample the posterior atmospheric CO_2 concentrations to the times and locations of the TCCON retrievals. TCCON is a network of ground-based Fourier transform spectrometers (FTS) that retrieve the column-average dry air mole faction of trace gases (e.g., CO_2 and CH_4; *Wunch et al*., 2011).We obtain the TCCON measurements from the TCCON Data Archive (http://tccondata.org/), and the TCCON retrievals are averaged to create 30-min average XCO_2 (e.g., *Crowell et al*., 2019).

Figs. S8-S12 depicts the biases and the RMSE between posterior XCO_2 and TCCON measurements across an array of sites; sites included in this study (Table S3) are similar to that in the OCO-2 inverse model inter-comparison (MIP) study (*Crowell et al*., 2019). Fig. S8 shows the comparisons across the entire study period, and Figs. S9-S12 each further show the comparisons for different seasons of the year. The biases are generally small across most of the sites (Fig. S8a) and are consistent across different seasons (Figs. S9 - S12), indicating an absence of any major seasonal biases in the inverse model estimates using OCO-2. With that said, the CalTech site exhibits higher biases than the other TCCON sites. The CalTech site is in the densely populated Los Angeles basin, a region that also has complex topography. We are unlikely to reproduce heterogeneous urban CO_2 signals given the spatial resolution of this global inverse model. Furthermore, the Eureka and Sodankyla sites exhibit higher biases than other TCCON sites. These sites are located at high latitudes where there are few observations from OCO-2 to constrain fluxes and posterior atmospheric CO_2 mixing ratios. The RMSE (Figs. S8-S12) ranges from 0.33 to 2.23 ppm at the different TCCON sites, which indicates that we can reproduce TCCON XCO_2 to within the range of uncertainties as described in the **R** covariance matrix (Sect. S1).

S5. Sensitivity tests for the estimated coefficients

We run the simulations with environmental driver datasets from two different meteorological products (CRUJRA and MERR-2) and two different formulations of the covariance matrix $\mathbf{\Psi}$ -- to test the sensitivity of the estimated coefficients to the choice of meteorology and statistical setup (Figs. S14 – S16). In Fig. S14, we compare estimated coefficients for the TBMs using environmental driver datasets from CRUJRA and MERRA-2 meteorology. The two sets of results look similar. In addition, Fig. S15 compares the coefficients estimated for OCO-2 observations using environmental driver datasets CRUJRA versus MERRA-2, and Fig. S16 compares coefficients estimated using different setups for the covariance matrix $\mathbf{\Psi}$. Note that the results in Figs. S15 and S16 are also shown in Figs. 3 and 4 of the main article, but the figures included here make the differences more visually apparent.

References

Basu, S., Baker, D.F., Chevallier, F., Patra, P.K., Liu, J.J. and Miller, J.B., 2018. The impact of transport model differences on CO2 surface flux estimates from OCO-2 retrievals of column average CO2.

Chevallier, F., Remaud, M., O'Dell, C.W., Baker, D., Peylin, P. and Cozic, A., 2019. Objective 4.1evaluation of surface-and satellite-driven carbon dioxide atmospheric inversions. *Atmospheric Chemistry and Physics*, *19*(22), pp.14233-14251.

Clark, D.B., Mercado, L.M., Sitch, S., Jones, C.D., Gedney, N., Best, M.J., Pryor, M., Rooney, G.G., Essery, R.L.H., Blyth, E. and Boucher, O., 2011. The Joint UK Land Environment Simulator (JULES), model description—Part 2: carbon fluxes and vegetation dynamics. *Geoscientific Model Development*, *4*(3), pp.701-722.

Cooperative Global Atmospheric Data Integration Project, 2019. Multi-laboratory compilation of atmospheric carbon dioxide data for the period 1957-2018; obspack_co2_1_GLOBALVIEWplus_v5.0_2019_08_12; NOAA Earth System Research Laboratory, Global Monitoring Division http://dx.doi.org/10.25925/20190812.

Crowell, S., Baker, D., Schuh, A., Basu, S., Jacobson, A.R., Chevallier, F., Liu, J., Deng, F., Liang, F., McKain, K. and Chatterjee, A., 2019. The 2015–2016 carbon cycle as seen from OCO-2 and the global in situ network. *Atmospheric Chemistry and Physics*, *19*(15), pp.9797-9831.

Deutscher, N., Notholt, J., Messerschmidt, J., Weinzierl, C., Warneke, T., Petri, C., Grupe, P. and Katrynski, K., TCCON data from Bialystok. *Poland, Release GGG2014R2, TCCON data archive, hosted by CaltechDATA.*

De Maziere, M., Sha, M.K., Desmet, F., Hermans, C., Scolas, F., Kumps, N., Metzger, J.M., Duflot, V. and Cammas, J.P., 2014. TCCON data from Reunion Island (La Reunion), France, Release GGG2014R1. *TCCON data archive, hosted by CaltechDATA.*

Dubey, M., Parker, H., Henderson, B., Green, D., Butterfield, Z., Keppel-Aleks, G., Allen, N., Blavier, J.F., Roehl, C., Wunch, D. and Lindenmaier, R., 10. TCCON data from Manaus (BR), Release GGG2014. R0, *TCCON Data Archive, hosted by CaltechDATA.*

Feist, D.G., Arnold, S.G., John, N. and Geibel, M.C., 2014. TCCON data from Ascension Island, Saint Helena, Ascension and Tristan da Cunha, Release GGG2014R0. *TCCON data archive, hosted by CaltechDATA.*

Goll, D.S., Vuichard, N., Maignan, F., Jornet-Puig, A., Sardans, J., Peng, S., Sun, Y., Kvakić, M., Guimberteau, M., Guenet, B. and Zaehle, S., 2017. ORCHIDEE-CNP: Site-Scale Evaluation against Observations from a Soil Formation Chronosequence in Hawaii. *AGUFM*, *2017*, pp.B54C-05.

Gourdji, S.M., Mueller, K.L., Schaefer, K. and Michalak, A.M., 2008. Global monthly averaged CO_2 fluxes recovered using a geostatistical inverse modeling approach: 2. Results including auxiliary environmental data. *Journal of Geophysical Research: Atmospheres*, *113*(D21).

Gourdji, S.M., Hirsch, A.I., Mueller, K.L., Yadav, V., Andrews, A.E. and Michalak, A.M., 2010. Regional-scale geostatistical inverse modeling of North American CO 2 fluxes: a synthetic data study. *Atmospheric Chemistry & Physics*, *10*(13).

Gourdji, S.M., Mueller, K.L., Yadav, V., Huntzinger, D.N., Andrews, A.E., Trudeau, M., Petron, G., Nehrkorn, T., Eluszkiewicz, J., Henderson, J. and Wen, D., 2012. North American CO 2 exchange: Inter-comparison of modeled estimates with results from a fine-scale atmospheric inversion. *Biogeosciences*, *9*(1), pp.457-475.

Griffith, D.W.T., Deutscher, N., Velazco, V.A., Wennberg, P.O., Yavin, Y., Aleks, G.K., Washenfelder, R., Toon, G.C., Blavier, J.F., Murphy, C. and Jones, N., 2014a. TCCON data from Darwin, Australia, Release GGG2014R0. *TCCON Data Archive, hosted by CaltechDATA.*

Griffith, D.W.T., Velazco, V.A., Deutscher, N., Murphy, C., Jones, N., Wilson, S., Macatangay, R., Kettlewell, G., Buchholz, R.R. and Riggenbach, M., 2014b. TCCON data from Wollongong. *Australia*, *Release GGG2014R0, TCCON data archive, hosted by CaltechDATA.*

Halko, N., Martinsson, P.G. and Tropp, J.A., 2011. Finding structure with randomness: Probabilistic algorithms for constructing approximate matrix decompositions. *SIAM review*, *53*(2), pp.217-288.

Haverd, V., Smith, B., Nieradzik, L., Briggs, P.R., Woodgate, W., Trudinger, C.M., Canadell, J.G. and Cuntz, M., 2018. A new version of the CABLE land surface model (Subversion revision r4601) incorporating land use and land cover change, woody vegetation demography, and a novel optimisation-based approach to plant coordination of photosynthesis. *Geoscientific Model Development*, *11*, pp.2995-3026.

Hase, F., Blumenstock, T., Dohe, S., Groß, J., & Kiel, M. (2014). TCCON data from Karlsruhe. *Germany, Release GGG2014R1, TCCON data archive, hosted by CaltechDATA.*

Iraci, L.T., Podolske, J., Hillyard, P.W., Roehl, C., Wennberg, P.O., Blavier, J.F., Allen, N., Wunch, D., Osterman, G. and Albertson, R., TCCON data from Edwards (US), Release GGG2014. R1, *TCCON Data Archive, hosted by CaltechDATA.*

Heskel, M.A., O'Sullivan, O.S., Reich, P.B., Tjoelker, M.G., Weerasinghe, L.K., Penillard, A., Egerton, J.J., Creek, D., Bloomfield, K.J., Xiang, J. and Sinca, F., 2016. Convergence in the temperature response of leaf respiration across biomes and plant functional types. *Proceedings of the National Academy of Sciences*, *113*(14), pp.3832-3837.

Jacobson, A.R., Schuldt, K.N., Miller, J.B., Oda, T., Tans, P., Andrews, A., Mund, J., Ott, L. and Zimnoch, M., 2020. CarbonTracker CT2019. *NOAA Earth System Research Laboratory, Global Monitoring Division*.

Joetzjer, E., Delire, C., Douville, H., Ciais, P., Decharme, B., Carrer, D., Verbeeck, H., De Weirdt, M. and Bonal, D., 2015. Improving the ISBA (CC) land surface model simulation of water and carbon fluxes and stocks over the Amazon forest. *Geoscientific Model Development*, *8*(6), pp.1709-1727.

Kato, E., Kinoshita, T., Ito, A., Kawamiya, M. and Yamagata, Y., 2013. Evaluation of spatially explicit emission scenario of land-use change and biomass burning using a process-based biogeochemical model. *Journal of Land Use Science*, *8*(1), pp.104-122.

Kawakami, S., Ohyama, H., Arai, K., Okumura, H., Taura, C., Fukamachi, T. and Sakashita, M., TCCON data from Saga. *Japan, Release GGG2014R0. TCCON data archive, hosted by CaltechDATA.*

Kivi, R. and Heikkinen, P., 2016. Fourier transform spectrometer measurements of column CO_2 at Sodankylä, Finland. *Geoscientific Instrumentation, Methods and Data Systems*, *5*(2), pp.271-279.

Krinner, G., Viovy, N., de Noblet-Ducoudré, N., Ogée, J., Polcher, J., Friedlingstein, P., Ciais, P., Sitch, S. and Prentice, I.C., 2005. A dynamic global vegetation model for studies of the coupled atmosphere-biosphere system. *Global Biogeochemical Cycles*, *19*(1).

Lienert, S. and Joos, F., 2018. A Bayesian ensemble data assimilation to constrain model parameters and land-use carbon emissions. *Biogeosciences*, *15*(9), pp.2909-2930.

Liu, J., Baskaran, L., Bowman, K., Schimel, D., Bloom, A.A., Parazoo, N.C., Oda, T., Carroll, D., Menemenlis, D., Joiner, J. and Commane, R., 2020. Carbon Monitoring System Flux Net Biosphere Exchange 2020 (CMS-Flux NBE 2020). *Earth System Science Data Discussions*, pp.1-53.

Liu, D.C. and Nocedal, J., 1989. On the limited memory BFGS method for large scale optimization. *Mathematical programming*, *45*(1-3), pp.503-528.

Mahadevan, P., Wofsy, S.C., Matross, D.M., Xiao, X., Dunn, A.L., Lin, J.C., Gerbig, C., Munger, J.W., Chow, V.Y. and Gottlieb, E.W., 2008. A satellite-based biosphere parameterization for net ecosystem CO_2 exchange: Vegetation Photosynthesis and Respiration Model (VPRM). *Global Biogeochemical Cycles*, *22*(2).

Masarie, K.A., Peters, W., Jacobson, A.R. and Tans, P.P., 2014. ObsPack: a framework for the preparation, delivery, and attribution of atmospheric greenhouse gas measurements. *Earth Syst. Sci. Data*, *6*(2), pp.375-384.

Mauritsen, T., Bader, J., Becker, T., Behrens, J., Bittner, M., Brokopf, R., Brovkin, V., Claussen, M., Crueger, T., Esch, M. and Fast, I., 2019. Developments in the MPI-M Earth System Model version 1.2 (MPI-ESM1. 2) and its response to increasing CO_2. *Journal of Advances in Modeling Earth Systems*, *11*(4), pp.998-1038.

Meiyappan, P., Jain, A.K. and House, J.I., 2015. Increased influence of nitrogen limitation on CO_2 emissions from future land use and land use change. *Global Biogeochemical Cycles*, *29*(9), pp.1524-1548.

Melton, J.R. and Arora, V.K., 2016. Competition between plant functional types in the Canadian Terrestrial Ecosystem Model (CTEM) v. 2.0. *Geoscientific Model Development*, *9*(1), p.323.

Miller, S.M., Miller, C.E., Commane, R., Chang, R.Y.W., Dinardo, S.J., Henderson, J.M., Karion, A., Lindaas, J., Melton, J.R., Miller, J.B. and Sweeney, C., 2016. A multiyear estimate of methane fluxes in Alaska from CARVE atmospheric observations. *Global biogeochemical cycles*, *30*(10), pp.1441-1453.

Miller, S.M., Michalak, A.M., Yadav, V. and Tadić, J.M., 2018. Characterizing biospheric carbon balance using CO 2 observations from the OCO-2 satellite. *Atmospheric Chemistry and Physics*, *18*(9), pp.6785-6799.

Miller, S.M., Saibaba, A.K., Trudeau, M.E., Mountain, M.E. and Andrews, A.E., 2020. Geostatistical inverse modeling with very large datasets: an example from the Orbiting Carbon Observatory 2 (OCO-2) satellite. *Geoscientific Model Development*, *13*(3).

Morino, I., Matsuzaki, T. and Horikawa, M., 2016. TCCON data from Tsukuba (JP), 125HR, Release GGG2014. R2, *TCCON Data Archive, hosted by CaltechDATA.*

Mueller, K.L., Gourdji, S.M. and Michalak, A.M., 2008. Global monthly averaged CO2 fluxes recovered using a geostatistical inverse modeling approach: 1. Results using atmospheric measurements. *Journal of Geophysical Research: Atmospheres*, *113*(D21).

NOAA Carbon Cycle Group ObsPack Team, 2018. INPE atmospheric carbon dioxide data for the period 2015-2017; obspack_CO_2_1_INPE_RESTRICTED_v2.0_2018-11-13; NOAA Earth System Research Laboratory, Global Monitoring Division.

Notholt, J., Petri, C., Warneke, T., Deutscher, N., Buschmann, M., Weinzierl, C., Macatangay, R. and Grupe, P., 2014. TCCON data from Bremen, *Release GGG2014.R0, TCCON Data Archive, hosted by CaltechDATA.*

Oleson, K.W., Lawrence, D.M., Bonan, G.B., Drewniak, B., Huang, M., Koven, C.D., Levis, S., Li, F., Riley, W.J., Subin, Z.M. and Swenson, S.C., 2013. Technical description of version 4.5 of the Community Land Model (CLM), NCAR Technical Note: NCAR/TN-503+ STR. *National Center for Atmospheric Research (NCAR), Boulder, CO, USA, https://doi. org/10.5065/D6RR1W7M*.

Peters, W., Jacobson, A.R., Sweeney, C., Andrews, A.E., Conway, T.J., Masarie, K., Miller, J.B., Bruhwiler, L.M., Pétron, G., Hirsch, A.I. and Worthy, D.E., 2007. An atmospheric perspective on North American carbon dioxide exchange: CarbonTracker. *Proceedings of the National Academy of Sciences*, *104*(48), pp.18925-18930.

Poulter, B., Frank, D.C., Hodson, E.L. and Zimmermann, N.E., 2011. Impacts of land cover and climate data selection on understanding terrestrial carbon dynamics and the CO_2 airborne fraction. *Biogeosciences*, *8*, pp.2027-2026.

Sherlock, V., Connor, B., Robinson, J., Shiona, H., Smale, D. and Pollard, D.F., 2014. TCCON data from Lauder (NZ), 125HR, Release GGG2014. R0. *TCCON data archive, hosted by CaltechDATA.*

Strong, K., Mendonca, J., Weaver, D., Fogal, P., Drummond, J.R., Batchelor, R. and Lindenmaier, R., 2014. TCCON data from Eureka, Canada, Release GGG2014R3. *TCCON data archive, hosted by CaltechDATA.*

Sweeney, C., Karion, A., Wolter, S., Newberger, T., Guenther, D., Higgs, J.A., Andrews, A.E., Lang, P.M., Neff, D., Dlugokencky, E. and Miller, J.B., 2015. Seasonal climatology of CO_2 across North America from aircraft measurements in the NOAA/ESRL Global Greenhouse Gas Reference Network. *Journal of Geophysical Research: Atmospheres*, *120*(10), pp.5155-5190.

Tian, H., Chen, G., Lu, C., Xu, X., Hayes, D.J., Ren, W., Pan, S., Huntzinger, D.N. and Wofsy, S.C., 2015. North American terrestrial CO_2 uptake largely offset by CH_4 and N_2O emissions: toward a full accounting of the greenhouse gas budget. *Climatic Change*, *129*(3-4), pp.413-426.

Warneke, T., Messerschmidt, J., Notholt, J., Weinzierl, C., Deutscher, N., Petri, C., Grupe, P., Vuillemin, C., Truong, F., Schmidt, M. and Ramonet, M., TCCON data from Orleans. *France, Release GGG2014R1, TCCON data archive, hosted by CaltechDATA.*

Walker, A.P., Quaife, T., van Bodegom, P.M., De Kauwe, M.G., Keenan, T.F., Joiner, J., Lomas, M.R., MacBean, N., Xu, C., Yang, X. and Woodward, F.I., 2017. The impact of alternative trait-scaling hypotheses for the maximum photosynthetic carboxylation rate (Vcmax) on global gross primary production. *New Phytologist*, *215*(4), pp.1370-1386.

Wennberg, P.O., Roehl, C., Wunch, D., Toon, G.C., Blavier, J.F., Washenfelder, R., Keppel-Aleks, G., Allen, N. and Ayers, J., 2014. TCCON data from Park Falls (US), Release GGG2014. *R0. TCCON data archive, hosted by CaltechDATA.*

Wennberg, P.O., Wunch, D., Roehl, C.M., Blavier, J.F., Toon, G.C. and Allen, N.T., 2015. TCCON data from Caltech(US), Release GGG2014. R0. *TCCON data archive, hosted by CaltechDATA.*

Wofsy, S.C., Afshar, S., Allen, H.M., Apel, E., Asher, E.C., Barletta, B., Bent, J., Bian, H., Biggs, B.C., Blake, D.R. and Blake, N., 2018. ATom: Merged Atmospheric Chemistry, Trace Gases, and Aerosols, ORNL DAAC, Oak Ridge, Tennessee, USA.

Wunch, D., Wennberg, P.O., Toon, G.C., Connor, B.J., Fisher, B., Osterman, G.B., Frankenberg, C., Mandrake, L., O'Dell, C., Ahonen, P. and Biraud, S.C., 2011. A method for evaluating bias in global measurements of CO_2 total columns from space.

Zaehle, S. and Friend, A.D., 2010. Carbon and nitrogen cycle dynamics in the O-CN land surface model: 1. Model description, site-scale evaluation, and sensitivity to parameter estimates. *Global Biogeochemical Cycles*, *24*(1).

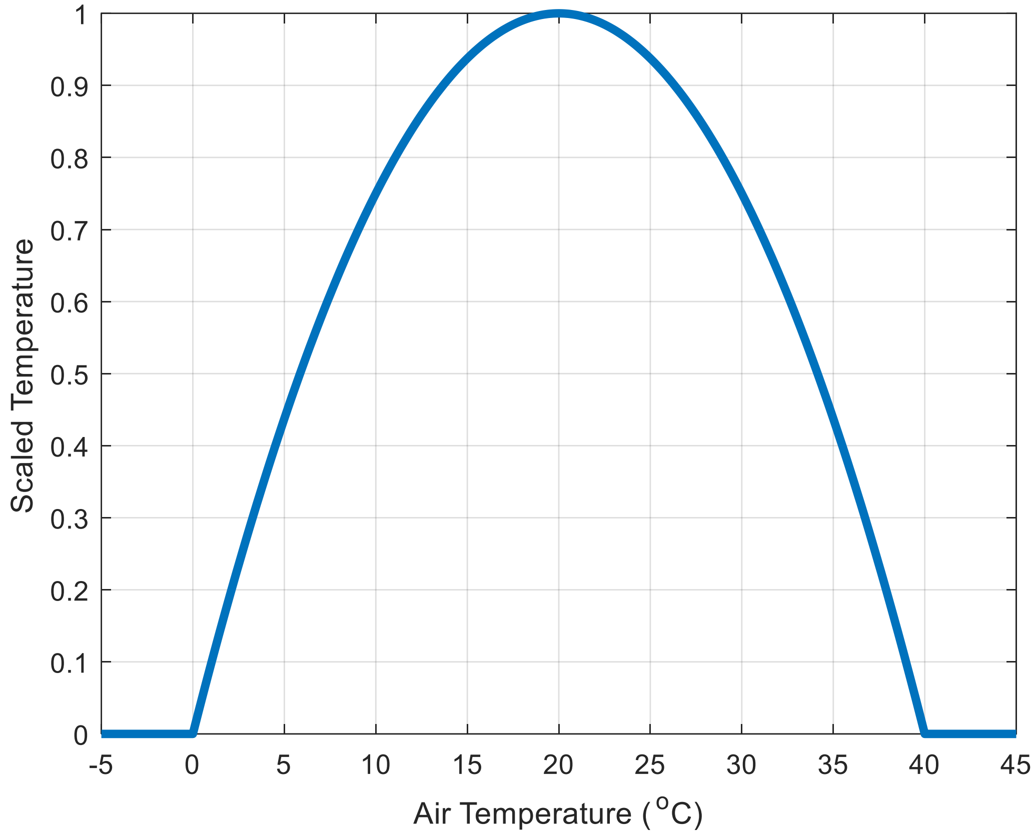

Figure S1. Scaled air temperature function for photosynthesis. This figure displays the function used for the temperate forest biome; the function has different optimal temperatures in different biomes.

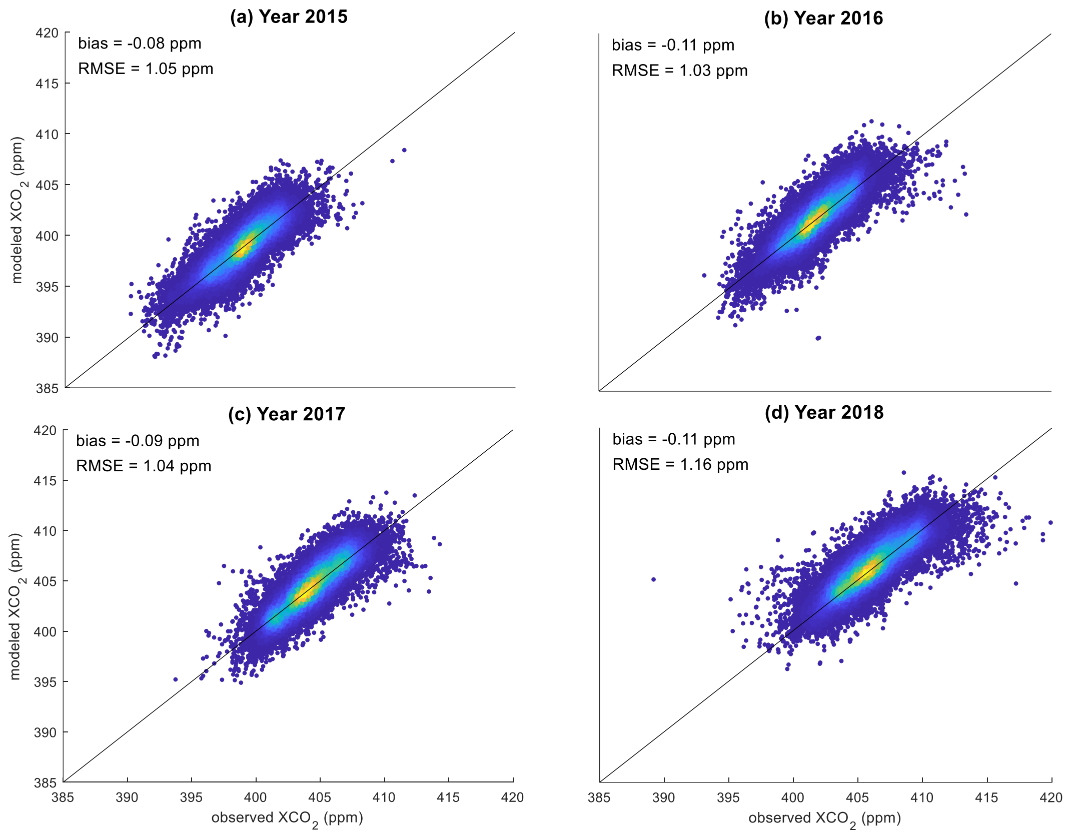

Figure S2. Comparisons against XCO_2 observations for years 2015 to 2018. Yellow and green colors indicate a high density of points while blue colors indicate a low density of data points.

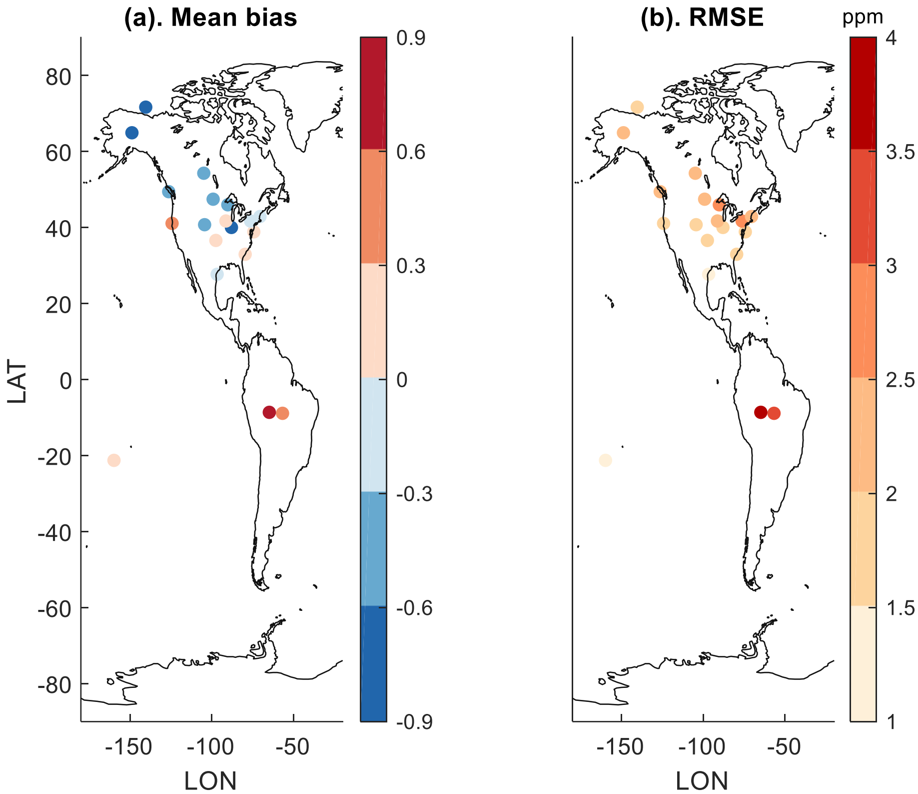

Figure S3. Site-level comparisons against measurements collected from NOAA regular sites and INPE sites (year 2015).

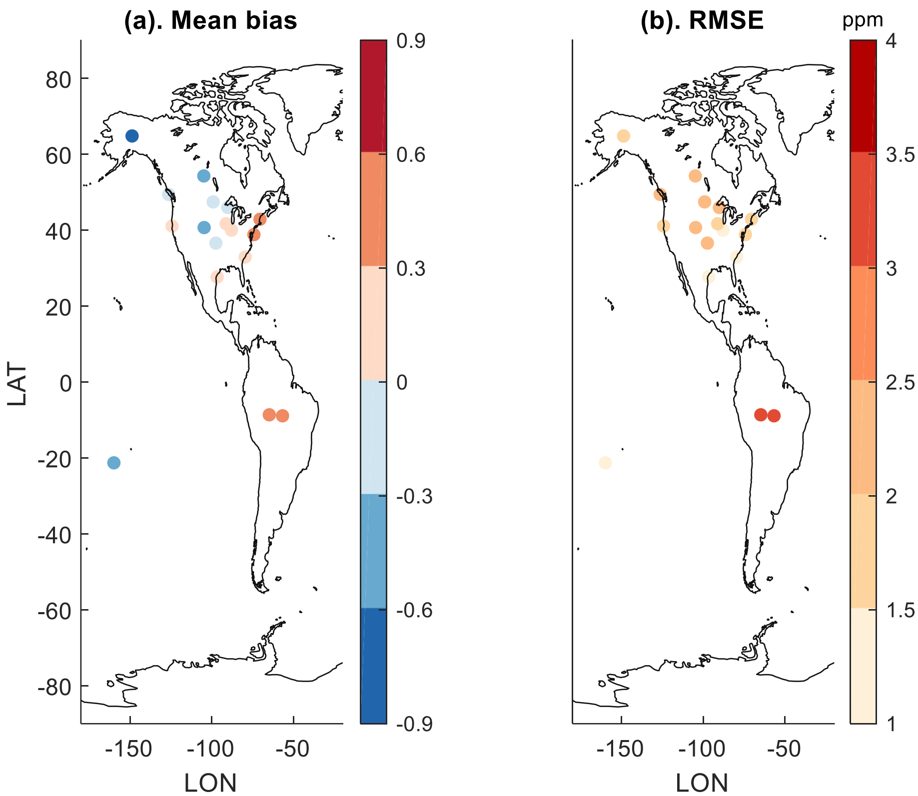

Figure S4. Site-level comparisons against measurements collected from NOAA regular sites and INPE sites (year 2016).

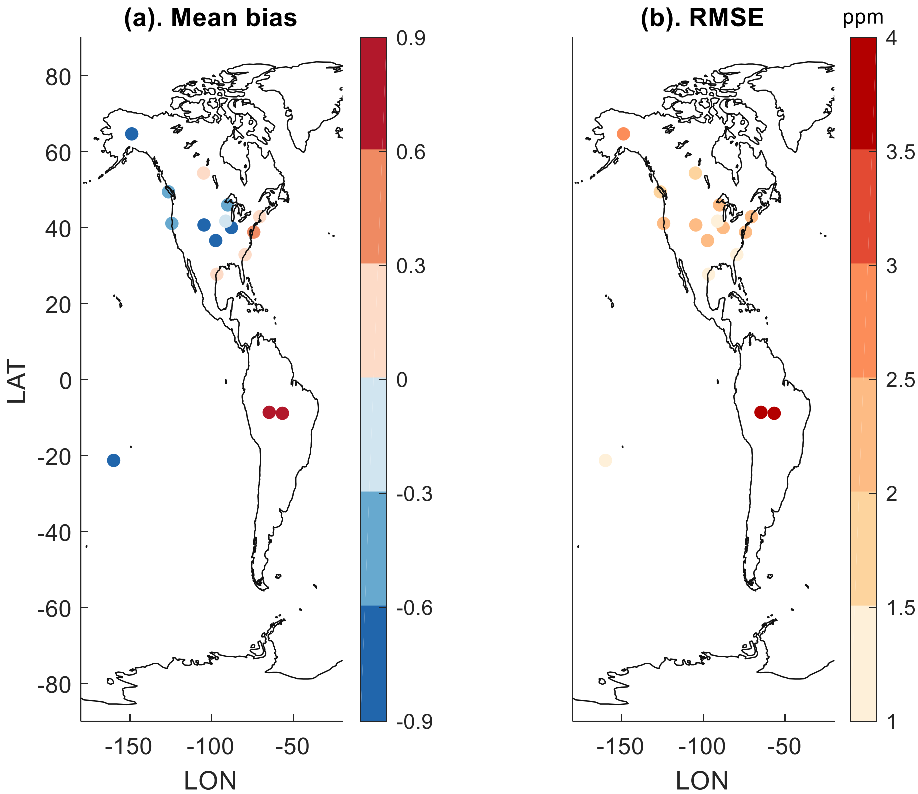

Figure S5. Site-level comparisons against measurements collected from NOAA regular sites and INPE sites (year 2017).

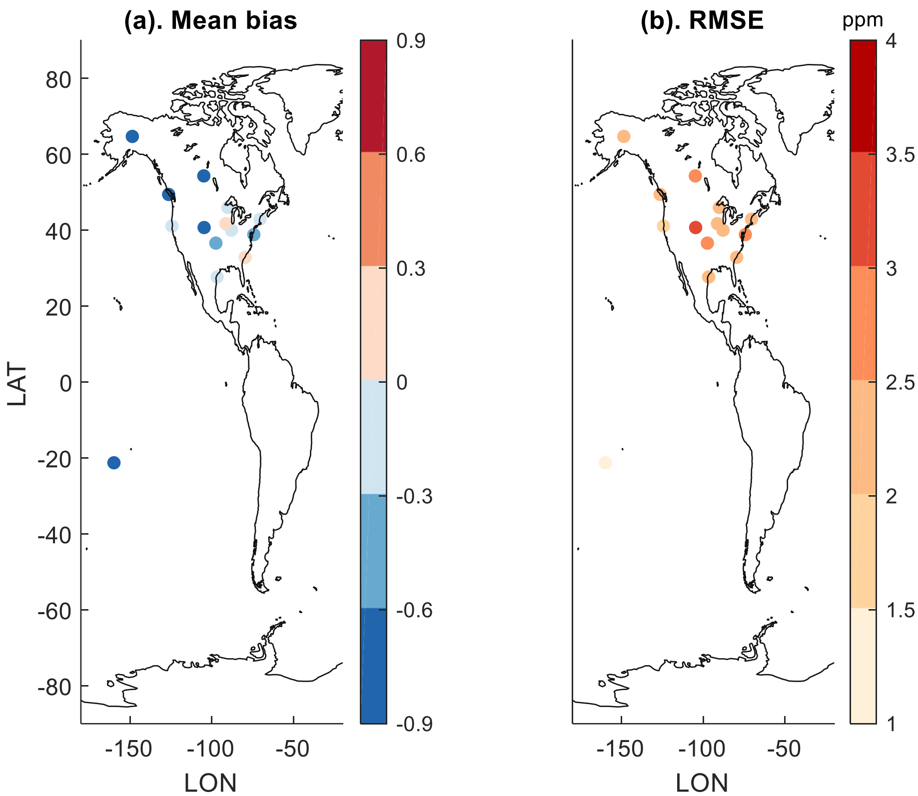

Figure S6. Site-level comparisons against measurements collected from NOAA regular sites and INPE sites (year 2018).

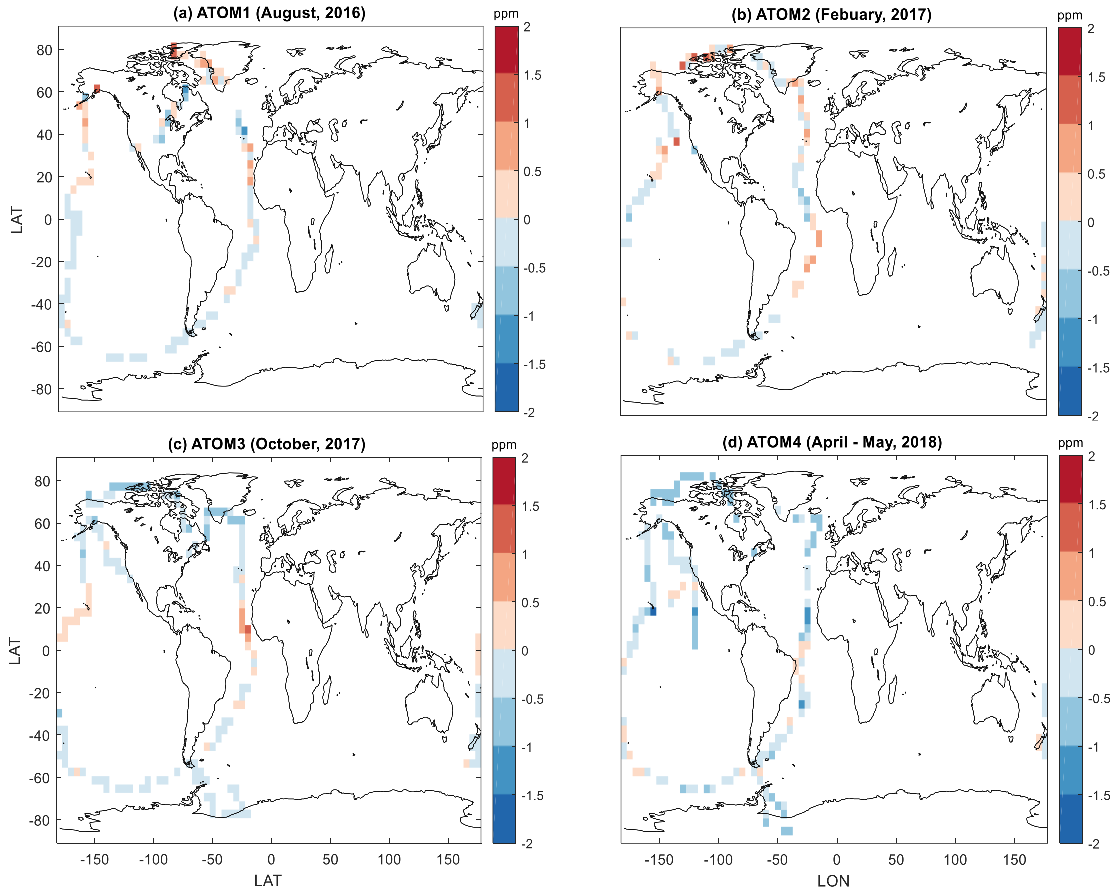

Figure S7. Grid-scale differences between the posterior CO_2 estimate and ATom aircraft measurements (model minus measurements).

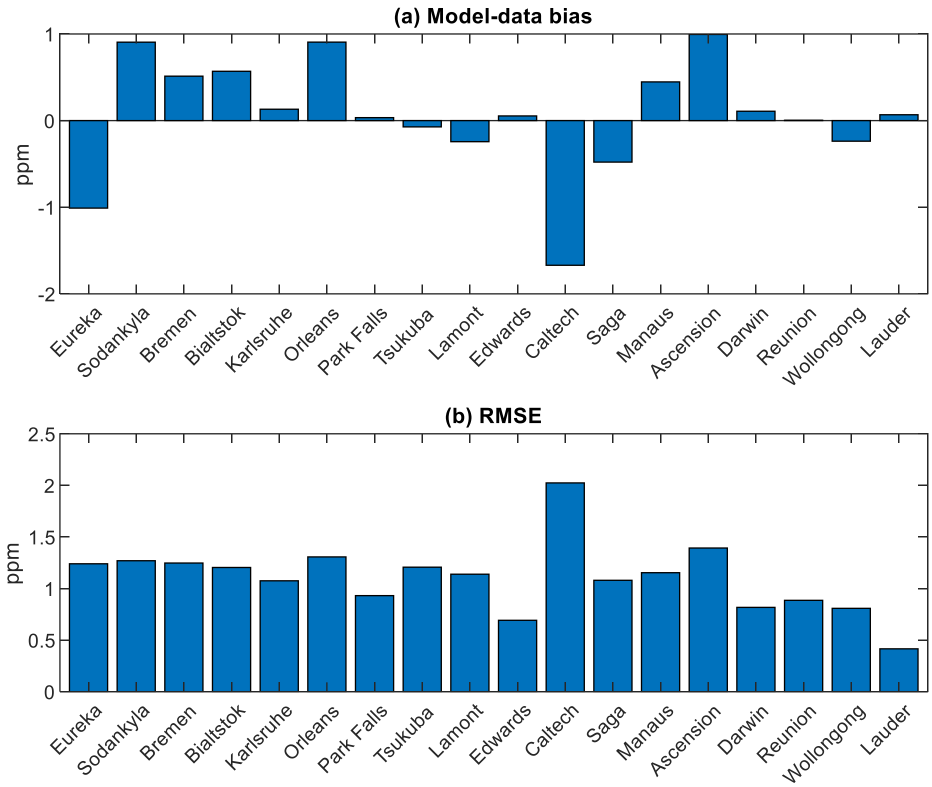

Figure S8. Comparisons between the posterior XCO_2 estimate and TCCON observations across years 2015-2018. We order these sites from Northern Hemisphere to Southern Hemisphere.

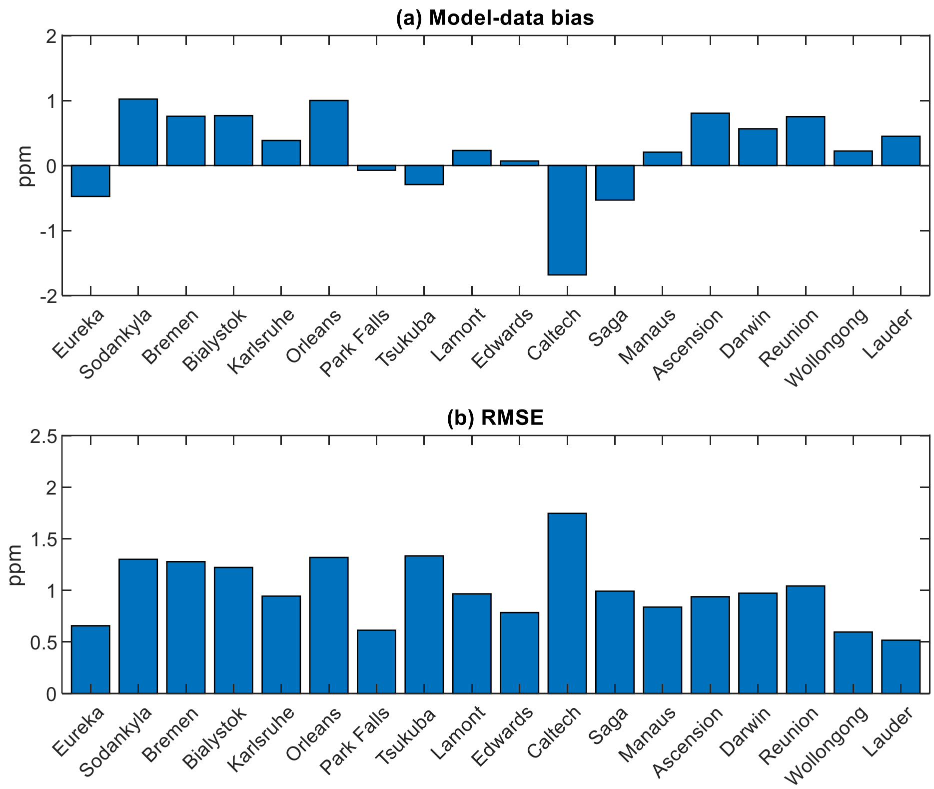

Figure S9. Comparisons between the posterior XCO_2 estimate and TCCON observations for March, April, and May (MAM) across the four-year study period.

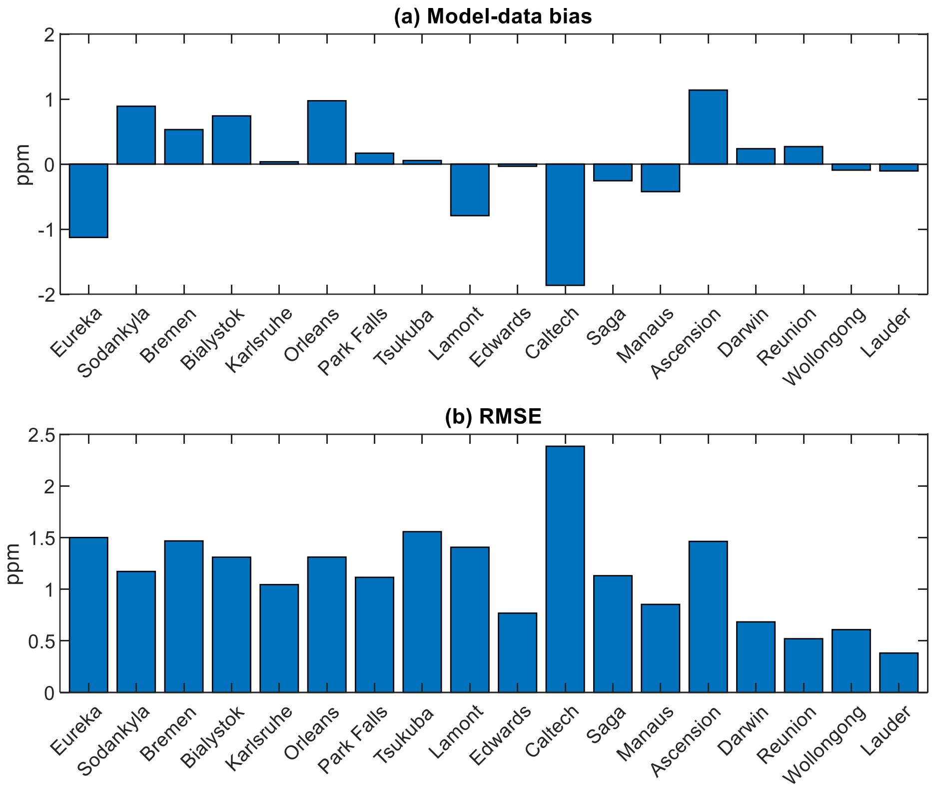

Figure S10. Comparisons between the posterior XCO_2 estimate and TCCON observations for June, July, and August (JJA) across the four-year study period.

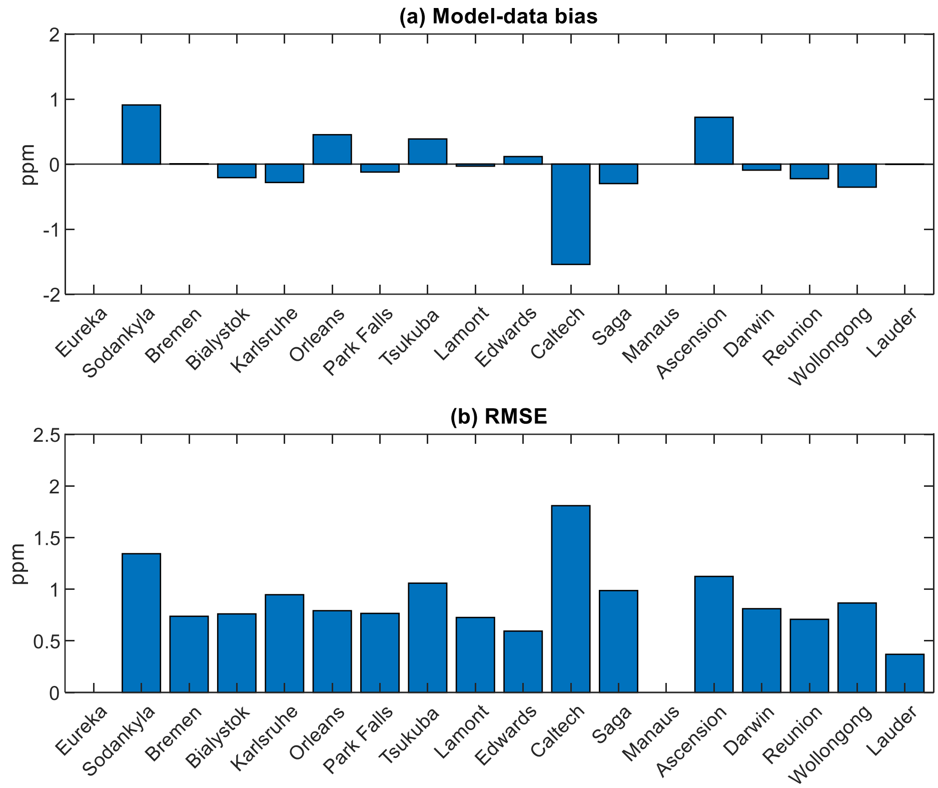

Figure S11. Comparisons between the posterior XCO_2 estimate and TCCON observations for September, October, and November (SON) across the four-year study period. Note the blank color indicates there are no available TCCON observations during SON over the individual sites. Also note that the model-data bias over Bremen and Lauder sites in panel (a) are small (0.005 and -0.004 ppm, respectively) but not blank.

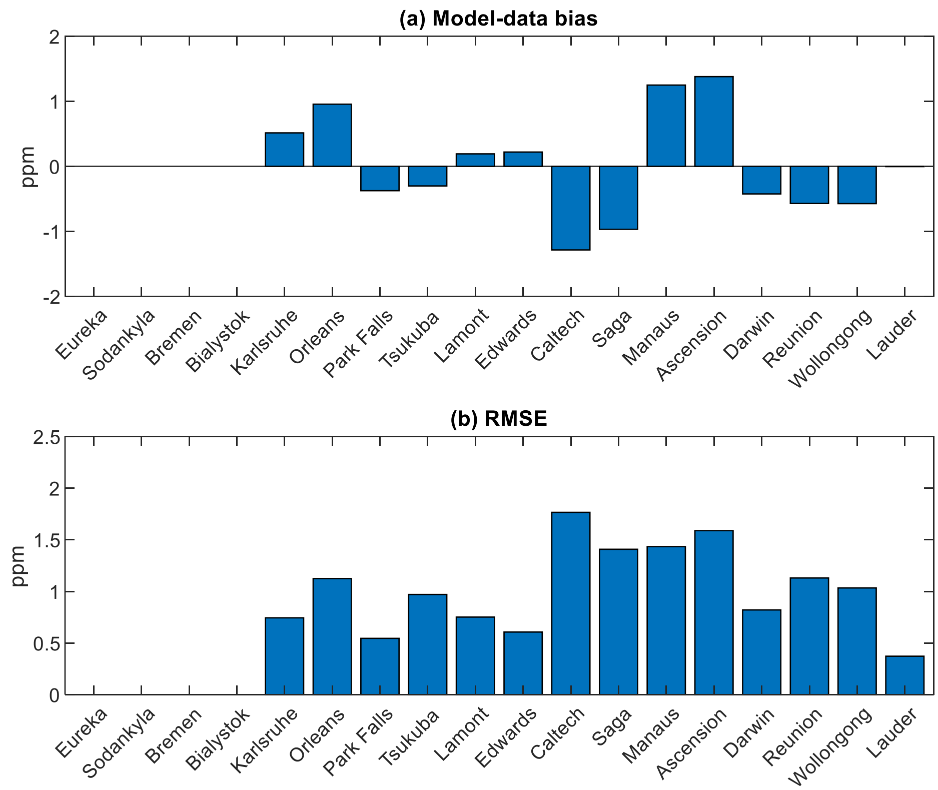

Figure S12. Comparisons between the posterior XCO_2 estimate and TCCON observations for December, January, and February (DJF) across the four-year study period. Note the blank color indicates there are not any available TCCON observations during DJF for the site in question.

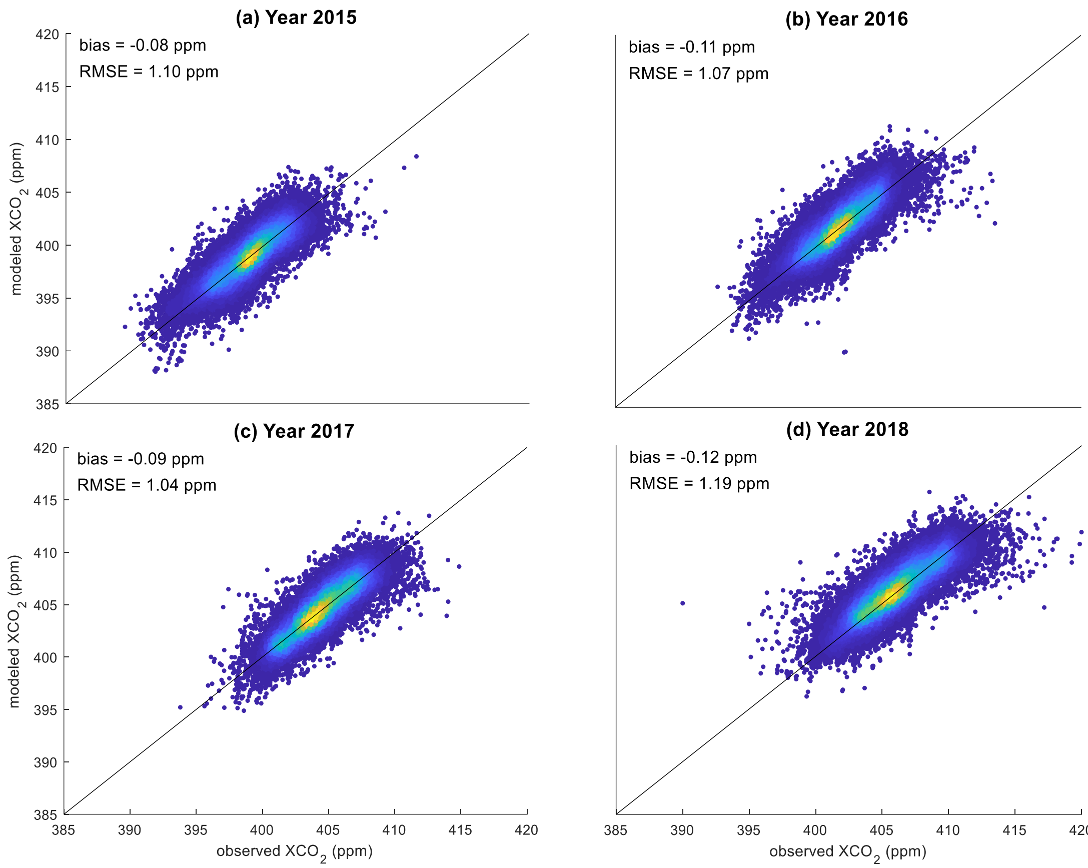

Figure S13. Comparison between modeled XCO_2 using the output of the regression analysis (***X*β**; Sect. 2) and XCO_2 observations for years 2015 to 2018. The biases (model minus observation) across years 2015-2018 are small (-0.12 to -0.08 ppm). The model-data residues are also within the range of uncertainties as described in the **R** covariance matrix (0.98 ± 0.31 ppm; see Sect. S1). In addition, the model-data residuals are similar from one year to another and do not display any trend.

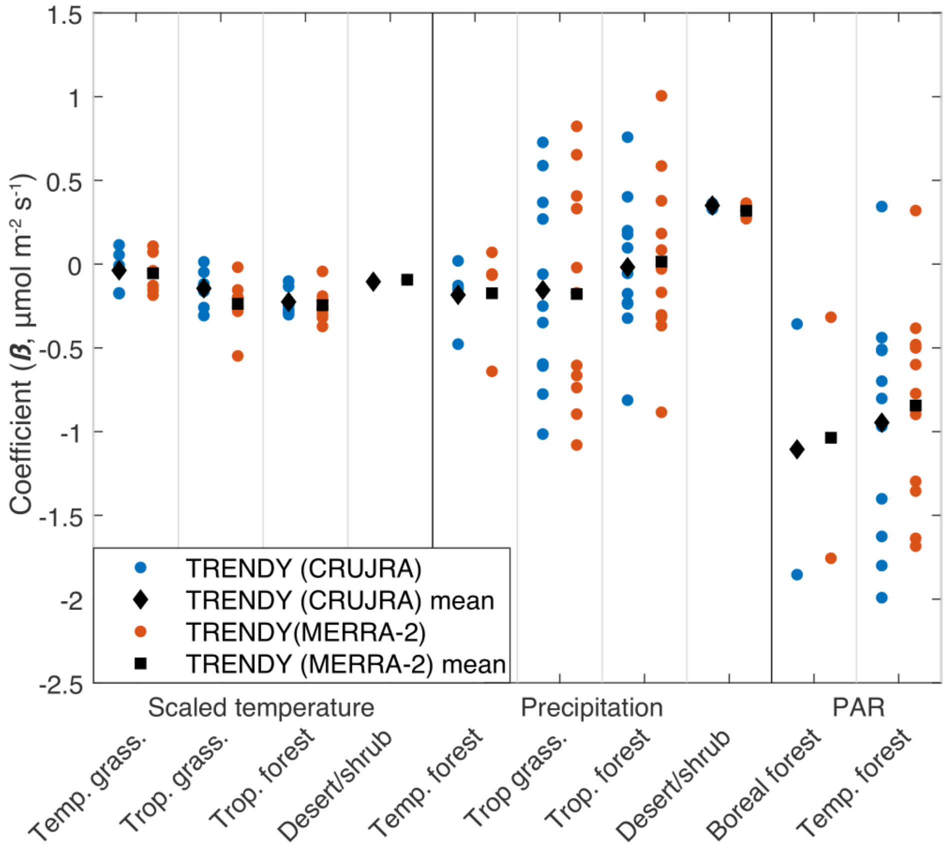

Figure S14. In the analysis using TBMs, we run simulations using CRUJRA (blue) and using MERRA-2 (red), respectively. The estimated coefficients between the two simulations are similar across different environmental drivers and across different biomes.

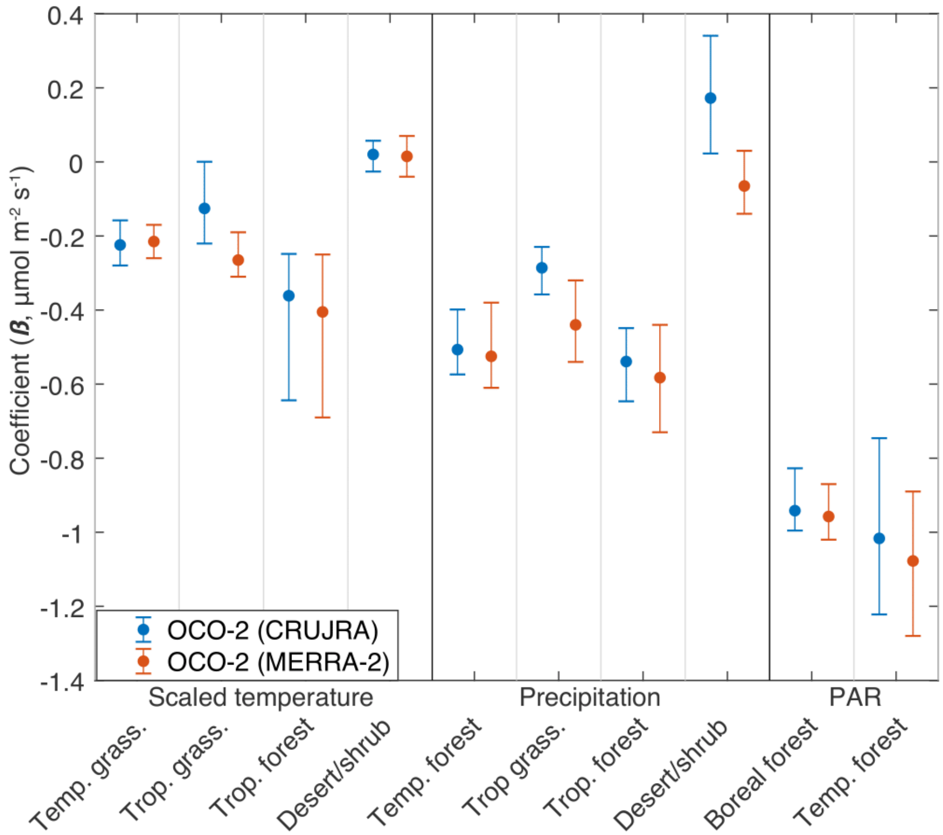

Figure S15. In the analysis using OCO-2, we run the simulations using environmental driver datasets from MERRA-2 (red) and from CRUJRA (blue). The vertical bars denote the range of coefficient estimates across four years and the dots denote the mean values. The estimated coefficients between the two simulations are similar for most environmental driver variables.

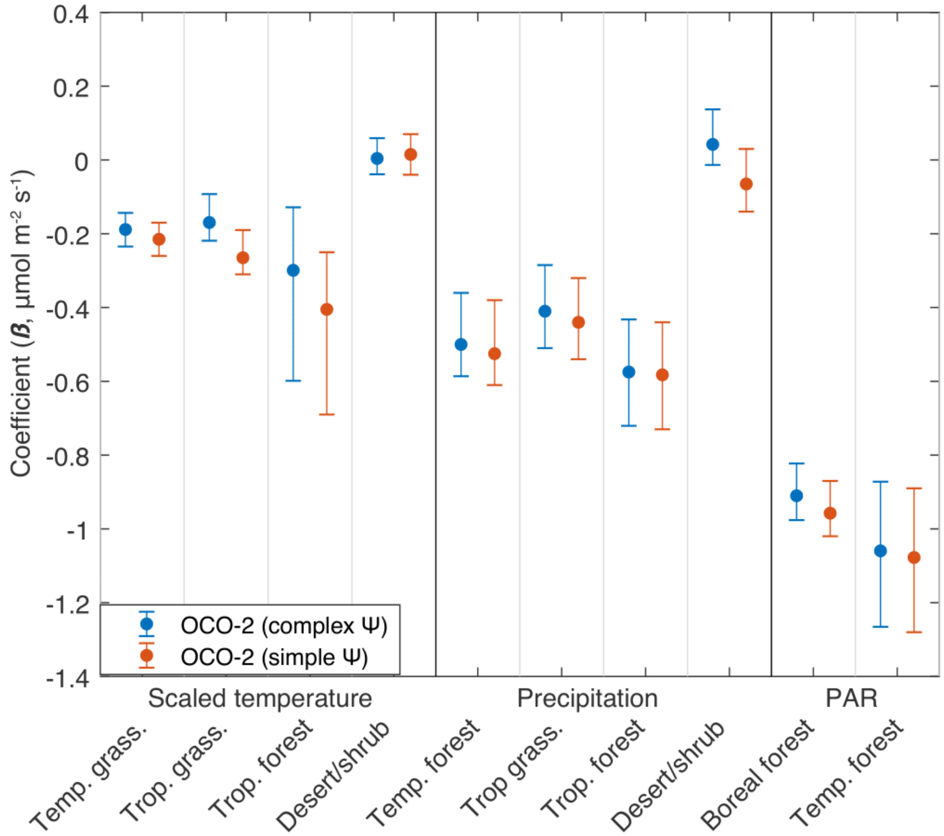

Figure S16. Comparison between the coefficients estimated using a simple, diagonal formulation of **Ψ** (red) and using a more complex and complete formulation of **Ψ** (blue). The vertical bars denote the range of coefficient estimates across four years and the dots denote the mean values.

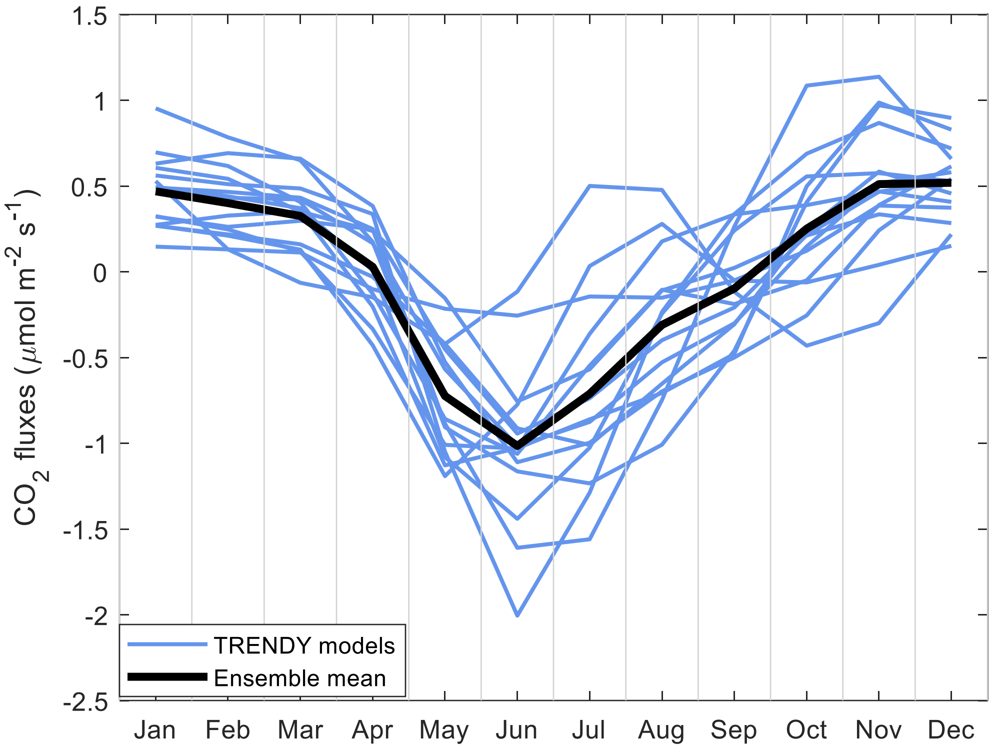

Figure S17. Four-year averaged CO_2 fluxes estimated from a suite of 15 TBMs (blue) and from the ensemble mean (black) for temperate forests. TBM disagree on the seasonality and the magnitude. These large differences of CO_2 fluxes over temperate forests likely help explain the large spread of coefficient estimates for PAR (Figs. 3a and 4).

Table S1. A full list of TBMs participating in TRENDY.

TRENDY models	Original spatial resolution	Reference
CABLE-POP	1°×1°	Haverd *et al.*, 2018
CLASS-CTEM	2.8125°×2.8125°	Melton and Arora, 2016
CLM5.0	1.25°×0.9424°	Oleson *et al.*, 2013
DLEM	0.5°×0.5°	Tian *et al.*, 2015
ISAM	0.5°×0.5°	Meiyappan *et al.*, 2015
JSBACH	1.875°×1.875°	Mauritsen *et al.*, 2019
JULES	1.875°×1.25°	Clark *et al.*, 2011
LPJ	0.5°×0.5°	Poulter *et al.*, 2011
LPX-Bern	0.5°×0.5°	Lienert and Joos, 2018
OCN	1°×1°	Zaehle and Friend, 2010
ORCHIDEE	2°×2°	Krinner *et al.*, 2005
ORCHIDEE-CNP	2°×2°	Goll *et al.*, 2017
SDGVM	1°×1°	Walker *et al.*, 2017
ISBA-CTRIP	1°×1°	Joetzjer *et al.*, 2015
VISIT	0.5°×0.5°	Kato *et al.*, 2013

Table S2. Aircraft measurements from NOAA regular sites, INPE sites, and ATom campaign.

site or program code	Site or program name	Network
ACG	Alaska Coast Guard, USA	NOAA/ESRL Global Greenhouse Gas Reference Network (e.g., *Sweeny et al*., 2015)
CAR	Briggsdale, Colorado, USA	
CMA	Offshore Cape May, New Jersey, USA	
CRV	CARVE	
DND	Dahlen, North Dakota, USA	
ESP	Estevan Point, British Columbia, Canada	
ETL	East Trout Lake, Saskatchewan, Canada	
HIL	Homer, Illinois, USA	
LEF	Park Falls, Wisconsin, USA	
MRC	Marcellus, Pennsylvania, USA	
NHA	Offshore Portsmouth, New Hampshire, USA	
PFA	Poker Flat, Alaska, USA	
RTA	Rarotonga, Cook Islands	
SCA	Offshore Charleston, South Carolina, USA	
SGP	Southern Great Plains, Oklahoma, USA	
TGC	Offshore Corpus Christi, Texas, USA	
THD	Trinidad Head, California, USA	
WBI	West Branch, Iowa, USA	
RBA_B	Rio Branco, Brazil	INPE
ALF	Alta Floresta, Brazil	
TOM	ATom, Atmospheric Tomography Mission	NASA Airborne Science (*Wofsy et al*., 2018)

Table S3. TCCON sites used in this study.

Site name	Reference
Park Falls, Wisconsin, USA	Wennberg et al. (2014)
Lamont, Oklahoma, USA	Wennberg et al. (2014)
Bialystok, Poland	Deutscher et al. (2015)
Orleans, France	Warneke et al. (2014)
Karlsuhe, Germany	Hase et al. (2015)
Tsukuba, Japan	Morino et al. (2016)
Lauder, New Zealand	Sherlock et al (2014)
Darwin, Australia	Griffith et al (2014a)
Wollongong, Australia	Griffith et al (2014b)
Bremen, Germany	Notholt et al (2014)
Eureka, Canada	Strong et al (2016)
Sodankyla, Finland	Kivi and Heikkinen (2016)
Reunion Island, France	De Maziere et al (2014)
Ascension Island, UK	Feist et al (2014)
Saga, Japan	Kawakami et al (2014)
Manaus, Brazil	Dubey et al (2014)
Caltech, California, USA	Wennberg et al (2015)
Edwards, California, USA	Iraci et al (2016)

Table S4. Estimated regression coefficients for the analysis using the TBMs and OCO-2 observations. In each box, we show the range of the coefficients, with the top and bottom values indicating the minimum and maximum coefficients, respectively, across years 2015 to 2018. Blank boxes indicate that the specific drivers are not selected in the individual TBMs. The environmental driver datasets shown in this table are those selected using real OCO-2 observations (as in Figs. 3-4). Note that for many TBMs, we also select additional environmental driver datasets that were not selected using real OCO-2 observations, and we do not list all of those coefficients in the table below for the sake of brevity.

TBMs or OCO-2 observations	Scaled temperature				Precipitation				PAR	
	Temp. grass.	Trop. Grass.	Trop. forest	Desert shrub	Temp. forest	Trop. Grass.	Trop. forest	Desert shrub	Boreal forest	Temp. forest
ISBA-CTRIP		-0.12, 0.16	-0.50, -0.17		-0.26, 0	-0.86, -0.54	-0.21, 0.030			-0.84, -0.32
DLEM	0.02, 0.11						-0.01, 0.28	0.19, 0.68		
LPX-Bern	-0.21, 0.07	-0.29, 0.05				-1.32, -0.91	-0.69, -0.06	0.23, 0.42		-1.97, -1.48
VISIT	0.09, 0.15	-0.44, -0.080	-0.18, 0.10			0.44, 0.84	0.14, 0.52	0.32, 0.47	-0.60, -0.10	0.22, 0.50
CABLE-POP			-0.33, -0.08				0.02, 0.26			
CLASS-CTEM				-0.15, -0.06		-0.45, -0.080	-0.44, -0.060			-0.68, -0.34
JSBACH		-0.43, 0.060	-0.56, 0.28		-0.25, 0.32	-0.36, 0.72	-0.07, 0.80			-2.08, -0.97
CLM5	-0.29, -0.10				-0.41, 0.22	-0.32, 0.52				-2.28, -0.99
JULES		-0.35, -0.080	-0.32, -0.08			0.68, 0.88	0.64, 1.25			-0.72, -0.58
OCN		-0.70, -0.14	-0.37, -0.21			0.17, 0.56				-0.57, -0.44
LPJ		-0.14, 0.060	-0.20 0			0.14, 0.52	0.54, 0.64			
SDGVM	-0.09, 0.04				-0.78, -0.23	-0.99, -0.69	-0.98, -0.73		-2.62 -1.47	-1.92, -1.15
ISAM			-0.39, -0.13			-0.76, -0.21	-0.24, 0.02			-0.90, -0.29
OECHIDEE-CNP	-0.19, -0.16	-0.19, 0.010								
ORCHIDEE		-0.28, 0.020	-0.41, -0.12			-0.80, -0.44	-0.42, -0.16			-1.11, -0.78
OCO-2	-0.28, -0.14	-0.31, 0	-0.69, -0.13	-0.04, 0.07	-0.61, -0.36	-0.54, -0.23	-0.73, -0.43	-0.14, 0.34	-1.02, -0.82	-1.28, -0.75